



The response of the migration of non-point source pollution to land use change in a typical small watershed in a semi-urbanized area



Yao Qian^{a,b,c}, Lang Sun^{a,b}, Dingkai Chen^a, Jiangfu Liao^d, Lina Tang^{a,*}, Qian Sun^a

^a Key Laboratory of Urban Environment and Health, Fujian Key Laboratory of Watershed Ecology, Institute of Urban Environment, Chinese Academy of Sciences, Xiamen 361021, China

^b University of Chinese Academy of Sciences, Beijing 100049, China

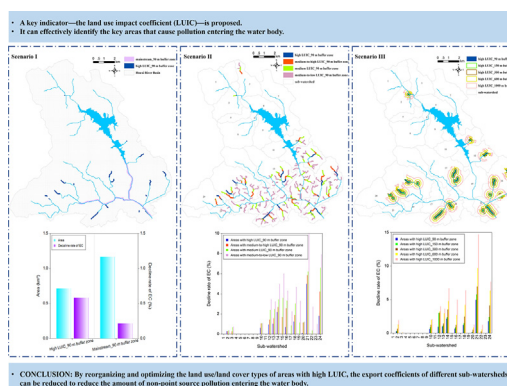
^c State Key Laboratory of Urban and Regional Ecology, Research Center for Eco-Environmental Sciences, Chinese Academy of Sciences, Beijing 100085, China

^d Computer Engineering College, Jimei University, Xiamen 361021, China

HIGHLIGHTS

- Export coefficient (EC) model is used to simulate migration path of NPS pollution.
- Land use impact coefficient (LUIC) is proposed to simulate land use affecting EC.
- LUIC helps to identify the key areas causing pollution to enter water bodies.
- Optimizing land use/cover in areas with high LUIC can effectively reduce ECs.

GRAPHICAL ABSTRACT



ARTICLE INFO

Article history:

Received 24 February 2021

Received in revised form 20 April 2021

Accepted 22 April 2021

Available online 28 April 2021

Editor: Fernando A.L. Pacheco

Keywords:

Export coefficient

Land use/land cover change

Non-point source pollution

Landscape index

Hydrological process

ABSTRACT

Land use change is one of the most important factors affecting the migration of non-point source (NPS) pollution. Watersheds in semi-urbanized areas are sensitive to human activities, especially the change of land use, which leads to significant changes in NPS pollution. In our research, by simulating the continuous dynamic migration path of NPS pollution in a typical small basin (Houxi River Basin) in a semi-urbanized area, a key indicator, namely the land use impact coefficient (LUIC), is proposed to explore the extent of the impact of land use on the export coefficient (EC) of NPS pollution. To reduce ECs, we set three scenarios for optimizing LUICs. The results show that: (1) Compared with the buffer zone in the mainstream of the river (1.16 km²), by optimizing land use/land cover types of areas with high LUIC (0.71 km²), the EC reduced by 0.58%, which is higher than that of reduced by 0.21%; (2) In terms of the sub-watersheds, the closer to the mainstream of the river, the more effective the reduction of EC by optimizing land use/land cover in areas with high LUIC; and (3) Compared with the ECs of areas with high LUIC under different buffer zone widths, the ECs of different LUIC values under a 90-meter buffer zone have a higher decline rate. Meanwhile, it is also necessary to consider the actual situation and reduce the costs of greening by selecting appropriate buffer zone areas. The significance of this research is that the proposed method is conducive to rapidly identifying the key areas of land use affecting the migration of NPS pollution. Through the rational planning of green space, it is possible to reduce ECs and lay a research foundation for proposing targeted land management, regional spatial planning, and strategies for the protection of basin ecological environments.

© 2021 Elsevier B.V. All rights reserved.

* Corresponding author.

E-mail address: Lintang@iue.ac.cn (L. Tang).

1. Introduction

Surface water in a basin is subject to significant risk due to rapid urbanization, including the emission and accumulation of NPS pollution related to population growth, industrial development, and the expansion of construction land (Yan et al., 2018). This not only endangers individuals, populations, and communities, but also has an adverse impact on ecological services (Tang et al., 2018). Therefore, most studies evaluate the degree of NPS pollution from the perspective of traceability, hydrological processes, and influencing factors so as to reduce the negative impact of such pollution.

There are two common hydrological model classifications, one is based on the spatial characteristics of the watershed, which can be divided into distributed models and lumped models. Another is based on the physical process, which can be divided into conceptual models and physical mechanism models. Distributed models usually contain several physical mechanism models, and lumped models usually contain several conceptual models. In recent years, distributed hydrological models have been widely used, such as SWAT, IHDM, SHE, and VIC. The advantage of these types of models lies in their strong applicability. The continuous and dynamic equations accurately describe the hydrological cycle process, while the model parameters have clear physical meanings which reflect the spatial characteristics of the watershed (Xu, 2009). However, these models are limited by data acquisition in parameter calibration, and also by the scaling effect, especially between sub-watersheds. For example, Ongley et al. (2010) showed that the runoff calibration of SWAT can be applied at the watershed scale (i.e., at a large scale); however, it cannot be determined whether the different land use types upstream of the gauging station contribute to the correct runoff values for each land use type. That is, the current SWAT model fails to characterize the contribution of different land use types to pollutants when they migrate from the surface to a water body.

Lumped models include lots of conceptual models, which regard the whole watershed as an independent calculation unit. Using statistics, the mathematical relationship between the influencing factors and NPS pollution (usually characterized by concentration) can be established, and the pollution load can also be estimated. The advantages of lumped models lie in their simplicity and practicality. For example, the non-point source pollution export coefficient (EC) method can be used to estimate the pollutant loads of different land use types (Beaulac and Reckhow, 1982; Johnes, 1996; Loehr et al., 1989; Shrestha et al., 2008). Furthermore, the multiple regression method was used to determine the organic matter/nutrient output coefficients of the main land use types in a basin (Hodge and Armstrong, 1993; McFarland and Hauck, 1998). Additionally, Shrestha and Kazama (2006) developed an empirical source contribution model to estimate the relative contribution of point source and non-point source loadings of organic matter and nutrients in the basin. Meanwhile, White et al. (2015) applied a stochastic sampling methodology loosely based on the Monte Carlo technique to construct a database of 45 million SWAT simulations which can be used to rapidly estimate nutrient loading for any small catchment in the United States for a given location, area, and land use distribution. Furthermore, Munafò et al. (2005) constructed a potential non-point pollution index to assess the global pressure exerted on rivers and other surface water bodies by different land uses, dividing the pressure of diffuse pollution coming from land units into three indexes, including land use, runoff, and distance from the river network. Wang et al. (2019) adopted the concept of dynamic time warping distances and developed a method for characterizing the differences in variation, information content, and similarity among time series of flow rate and agricultural NPS pollution loads at various sub-basin scales. Despite the fact that the method can identify the critical spatial scale of the basin, it is limited in that the spatial distribution of NPS pollution is presented in the form of clustering, which cannot be refined to a smaller scale.

To summarize, the limitation of conceptual models lies in the research method for the migration process of pollutants caused by surface runoff. Thus, many studies have researched the process of pollutant migration. Based on source-sink theory and landscape ecology, Chen (2015) proposed a method to simulate the migration of NPS pollution from the surface to a water body after rainfall runoff. They considered that the contribution of NPS pollution to water bodies is not only related to the pollution production capacity of each landscape unit but also to the ability of pollutants to migrate from the source to the receiving water body or water outlet. The advantage of their method is that it breaks the limitation of scale effect. The model belongs to the distributed hydrological model in terms of spatial characteristics, which also belongs to the conceptual hydrological model in terms of physical process. The model combines the advantages of the two models. On the one hand, some empirical functions are used to describe the complex hydrological process, which can simplify the simulation of NPS pollution migration process. On the other hand, the flow process of NPS pollution from upstream to downstream along each calculation unit when the basin is gridded, which is conducive to simulate the complete route of NPS pollution migration. Sun et al. (2018) developed a precipitation-weighted landscape structure model using the inequality function of the Lorenz curve to quantify the spatial structure of different landscape types, and then used the measured concentrations of nutrients (TN and TP) to validate the model and calculate the contributions of different land use types to the nutrient levels.

The change of land use structure and pattern has a significant impact on NPS pollution load (Zhang et al., 2013). Liang et al. (2020) considered that land use is the dominant factor affecting nutrient load, accounting for 50% of the relative importance. From the perspective of elasticity and watershed health, Ervinia et al. (2019) studied the coupled effects of climate variability and land use pattern on surface water quality. Meanwhile, Dai et al. (2017) found that the impact of land use type on river water quality is maximal in a buffer zone with a radius of 100–200 m and proposed that NPS pollution needs to be reduced in a zonal control based on the land function.

Many researchers agree that the best way to control NPS pollution is to increase forest land area and establish grassland buffer zones (Zhang et al., 2013; Zhang et al., 2018). However, it is unclear which locations are fit for establishing grassland buffer zones. Additionally, it is not certain what scale/size of buffer zone can most effectively mitigate the migration of NPS pollution into water bodies. Therefore, our study intended to conduct in-depth research to solve the questions mentioned above. The innovation of the research is that we put forward a key indicator to simulate the impact of land use on the EC of NPS pollution. By identifying key regions of the watershed, we can optimize the land use/land cover types or spatial layout in order to reduce the EC of NPS pollution.

2. Study area

The Houxi River Basin (HRB) is located close to Xiamen City, Fujian Province, China. It is located at 24°36′–24°45′N and 117°55′–118°4′E and covers an area of 138.7 km². The basin is a typical semi-urbanized area and its land use/land cover varies greatly. The northern region is dominated by forest, while the central and southern region contains large areas of agricultural land, construction land, and rural residential areas distributed in an alternating and crisscrossing pattern. In the HRB, the boundary between land use function and landscape pattern is not clear. With the radiation and diffusion of urban social and economic benefits, rural industrialization, and other factors, some rural areas with better location and endowment conditions in China have developed into semi-urbanized areas with mixed land use and rapid changes in socioeconomic structure (Liu et al., 2004). The rapid changes in land use/land cover in such semi-urbanized areas, such as the rapid expansion of construction land and the sharp decrease of forest land and cultivated land, have reduced the capacity of ecosystem services,

especially regulating services (e.g., water purification and waste disposal) and supporting services (e.g., habitat provision), which has led to the deterioration of surface water quality, the reduction of species diversity, and other negative ecological and environmental effects, which is not conducive to the coordinated development of regional economy and ecology (Fu et al., 2005; Huang et al., 2012).

We selected the HRB as the study area for the following reasons: on the one hand, the land use/land cover in the HRB watershed has changed greatly in the past decade (Fig. 1); on the other hand, excessive nitrogen and phosphorus fertilization have caused serious degradation of ecological and landscape functions. Therefore, the HRB was selected as a research object to explore the changes in the spatial distribution of NPS pollution caused by land use changes.

3. Methodology

3.1. Export coefficient of non-point source pollution

In the original concept of the EC proposed by Chen (2015), the EC was regarded as a landscape indicator based on ecological processes. This indicator can be used to perform the continuous dynamic simulation of the migration path of NPS pollution. This method is used to measure the ability of pollutants from various regions (usually represented by grids) to rivers during the migration of pollutants from the surface to the river, which is assumed to obey the “migration rules” (Zhao et al., 2010). These migration rules refer to the grid units in the watershed which are involved in the process of pollutant land–water migration based on the interaction of grid units. The contribution of each grid unit to pollutant output depends not only on the pollutants output by the runoff after rainfall but is also impelled by the inflow grids (i.e., the upslope grids) and hindered by subsequent flow through the

grids (i.e., the downslope grids). The simplified model can be written as follows:

$$a = c(1 + dm)(1 - b)^n \tag{1}$$

where a is the EC of the targeted grid, d is the dynamic coefficient, b is the resistance coefficient, m is the number of other grids flowing into the target grid, n is the number of grids that the target grid needs to pass through to flow into the outlet or into the receiving water body, and c is a constant.

Based on comprehensive consideration of the effects of land use, terrain, soil, rainfall, and other factors, Eq. (1) can be expanded, as shown in Eq. (2). Chen (2015) suggested that the relationship between Manning’s roughness coefficient and the hydrological velocity can be used to characterize the resistance coefficient of pollutant migration. Xie et al. (2005) calculated that Manning’s roughness coefficient is proportional to the 0.6 power of hydrological velocity. Therefore, the 0.6 power of the Manning’s roughness coefficient of different land use types is taken as the resistance coefficient. The dynamic coefficient is related to rainfall. After rainfall runoff, the potential energy of water flow is converted into kinetic energy, which promotes pollutant migration. The dynamic coefficient is characterized by the ratio of net rainfall depth to rainfall. Besides, based on the D8 algorithm, the flow direction can be determined in each grid.

$$a = c \left[1 + \sum_i^m d_i^{L_i} (1 + \theta_i^{0.3}) \right] \prod_j^n [(1 - b_j) \cdot (1 + \theta_j^{0.3})] \tag{2}$$

where L_i is the distance between the i th grid flowing into the target grid and the target grid, θ_i is the slope of the i th grid flowing into the target grid, and θ_j is the slope of the target grid flowing through the j th grid.

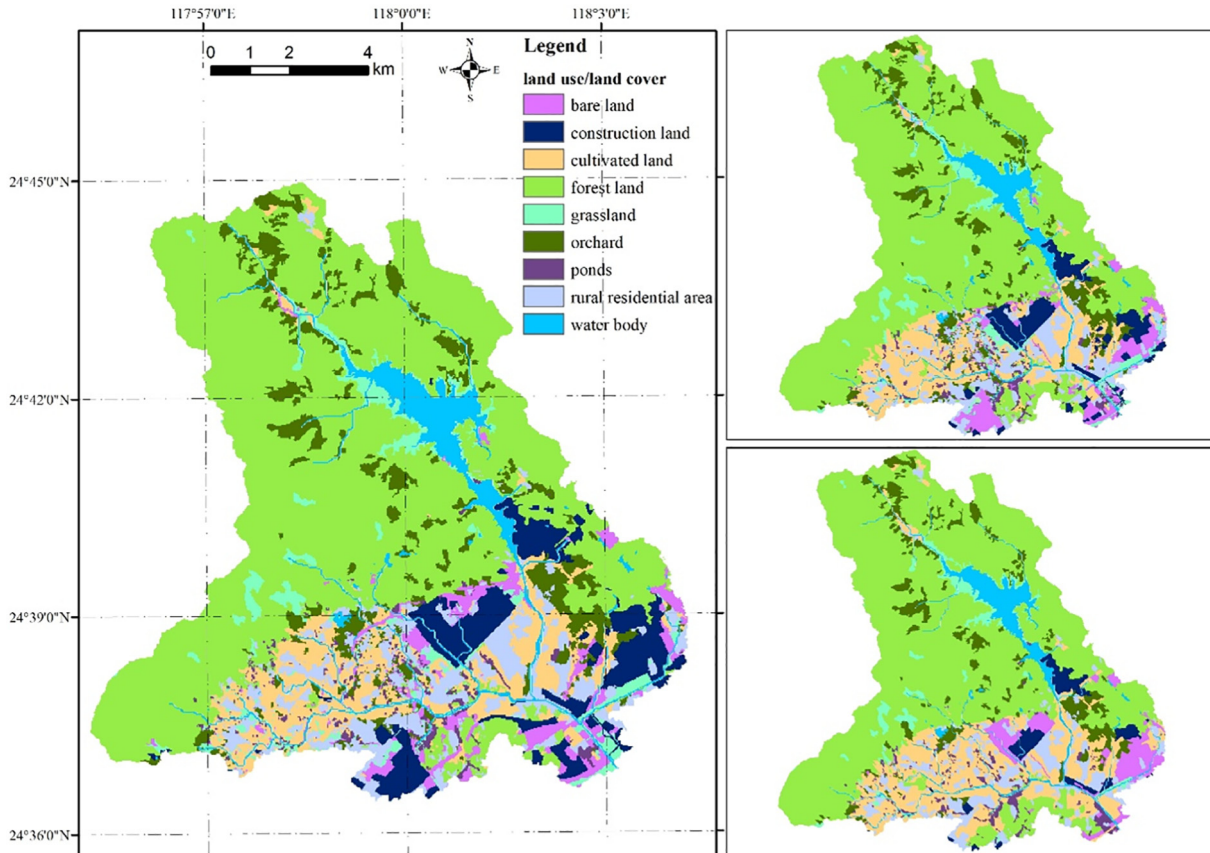


Fig. 1. Land use/land cover of the Houxi River Basin (HRB) in (a) 2019, (b) 2015, and (c) 2011.

In the research, the EC model has been improved, as shown in Eq. (3). It is suggested that in a certain water flow path, a certain target grid is affected by all upstream grids and affects all subsequent downstream grids. Therefore, in Eq. (2), the brackets in the expression $(1 - b_j)$ need to be deleted. Additionally, two constants, c_1 and c_2 , were added to the equation to ensure that the impact of the slope on the dynamic coefficient/resistance coefficient is between 0 and 1. Therefore, based on the improved EC model, we can compare the impacts of different land use/land cover simulation scenarios on the ECs.

$$a = \left[1 + \sum_i^m d_i^{\theta_i} (1 + c_1 \cdot \theta_i^{0.3}) \right] \prod_j^n [1 - b_j (1 + c_2 \cdot \theta_j^{0.3})] \quad (3)$$

where c_1 and c_2 are constants.

3.2. Land use impact coefficient

Although EC is affected by many factors, such as distance, land uses, slope, and rainfall, the climate and terrain factors of a certain watershed are relatively stable. At the same time, land uses are mainly affected by human activities, which means that the EC can be controlled and adjusted. From Eq. (3), the impact of land uses on EC is mainly reflected by the resistance coefficient (b). Therefore, to clarify the route of NPS pollution entering the river, we can reduce the number of ECs by optimizing the spatial layout of land use and rationally allocating land use types.

As shown in Fig. 2, it is assumed that the surface water flows from grid g_{13} to grids g_{23} , g_{32} , g_{43} , and g_{54} , and finally to grid g_{55} (water body). The EC of grid g_{13} is a_{13} , and the EC of grid g_{23} is a_{23} . The sum of ECs ($a_{13} + a_{23}$) can be regarded as a linear function with the resistance coefficient (b_{32}) of the target grid (g_{32}) as the independent variable (Eq. (10)). That is, the change of land use in a target grid (Δb) will cause a change in EC (ΔA). The land use impact coefficient (LUIC) is defined in Eq. (11). The larger the value of LUIC, the higher the influence of the grid on the EC. Therefore, adjusting the LUIC in the crucial/sensitive area of the watershed is beneficial to reducing the amount of pollutants entering the river.

The derivation process of LUIC is shown in Eqs. (4)–(13) below:

$$a_{23} = \left[1 + d_{13}^{\theta_{13}} (1 + c_1 \cdot \theta_{13}^{0.3}) \right] \cdot [1 - b_{43} (1 + c_2 \cdot \theta_{43}^{0.3})] \cdot [1 - b_{54} (1 + c_2 \cdot \theta_{54}^{0.3})] \cdot [1 - b_{32} (1 + c_2 \cdot \theta_{32}^{0.3})] \quad (4)$$

$$a_{23} = \left[1 + d_{13}^{\theta_{13}} (1 + c_1 \cdot \theta_{13}^{0.3}) \right] \cdot [1 - b_{43} (1 + c_2 \cdot \theta_{43}^{0.3})] \cdot [1 - b_{54} (1 + c_2 \cdot \theta_{54}^{0.3})] - \left[1 + d_{13}^{\theta_{13}} (1 + c_1 \cdot \theta_{13}^{0.3}) \right] \cdot [1 - b_{43} (1 + c_2 \cdot \theta_{43}^{0.3})] \cdot [1 - b_{54} (1 + c_2 \cdot \theta_{54}^{0.3})] \cdot (1 + c_2 \cdot \theta_{32}^{0.3}) \cdot b_{32} \quad (5)$$

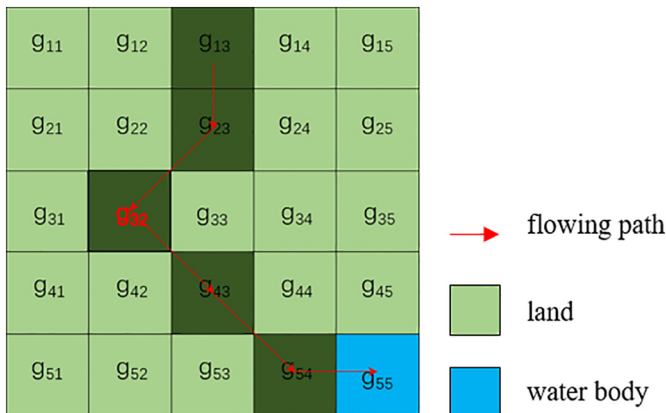


Fig. 2. Flowing path of surface water.

$$z_{23} = \left[1 + d_{13}^{\theta_{13}} (1 + c_1 \cdot \theta_{13}^{0.3}) \right] \cdot [1 - b_{43} (1 + c_2 \cdot \theta_{43}^{0.3})] \cdot [1 - b_{54} (1 + c_2 \cdot \theta_{54}^{0.3})] \quad (6)$$

$$k_{23} = \left[1 + d_{13}^{\theta_{13}} (1 + c_1 \cdot \theta_{13}^{0.3}) \right] \cdot [1 - b_{43} (1 + c_2 \cdot \theta_{43}^{0.3})] \cdot [1 - b_{54} (1 + c_2 \cdot \theta_{54}^{0.3})] \cdot (1 + c_2 \cdot \theta_{32}^{0.3}) \quad (7)$$

$$a_{23} = -k_{23} \cdot b_{32} + z_{23} \quad (8)$$

$$a_{13} = -k_{13} \cdot b_{32} + z_{13} \quad (9)$$

$$a_{13} + a_{23} = -(k_{13} + k_{23}) \cdot b_{32} + z_{13} + z_{23} \quad (10)$$

$$A_m = -K_m \cdot b_m + Z_m \quad (11)$$

$$A_m = a_1 + a_2 + \dots + a_n \quad (12)$$

$$K_m = k_1 + k_2 + \dots + k_n \quad (13)$$

where A_m is the sum of the ECs of the upstream grids which flow into the target grid, Z_m is a function related to the dynamic coefficient and the resistance coefficient, b_m is the resistance coefficient of the m th grid, n is the number of upstream grids flowing into the target grid, and K_m is the land use impact coefficient.

3.3. Scenario simulation of land use

3.3.1. Scenario I

Based on the land use situation in the HRB in 2019, optimizing the land use/land cover in areas with high LUIC and the areas around the mainstream of the Houxi River, we calculated the mitigation degree of EC in 2010 compared with that in 2019. In detail, we made a 90-meter buffer zone for areas with high LUIC values and the mainstream of the Houxi River, respectively, and then modified the type of land use in the buffer zone. When the buffer zone is in a non-urbanized area, it is set as a vegetation buffer zone (mainly forest/shrub grassland); meanwhile, when the buffer zone is in an urbanized area, it is set as urban green space (mainly grassland; Fig. 3).

3.3.2. Scenario II

The spatial distributions of the LUIC can be divided into five intervals, including (0–0.034], (0.034–0.13], (0.13–0.27], (0.27–0.46] and (0.46–0.98]. Based on the land use situation in the HRB in 2019, optimizing the land use/land cover in areas with high LUIC (0.46–0.98), areas with medium-to-high LUIC (0.27–0.46], areas with medium LUIC (0.13–0.27], and areas with medium-to-low LUIC (0.034–0.13], the influence of different LUIC values on the EC was calculated, and then the mitigation degree of EC in 2010 compared with that in 2019 was calculated. The settings of the land use change in the buffer zone were the same as in Scenario I (Fig. 4).

3.3.3. Scenario III

Based on the land use situation in the HRB in 2019, we analyzed different levels of buffers in areas with high LUIC values areas in the watershed, that is, to optimize land use types for different buffer zone widths (90, 150, 300, 600, and 1000 m), and then calculated the mitigation degree of EC in 2010 compared with that in 2019. The settings of the land use change in the buffer zone were the same as in Scenario I (Fig. 5).

Additionally, it should be noted that, if the buffer zone covers forest land, the type of land covered by the forest land is not replaced by grassland, while if the buffer zone originally covers grassland, the original grassland will not be calculated in the total change areas.

3.4. Data and preprocessing

The following data were required to calculate the LUIC: land use/land cover, topography, meteorology, soil, etc. (1) Remote sensing

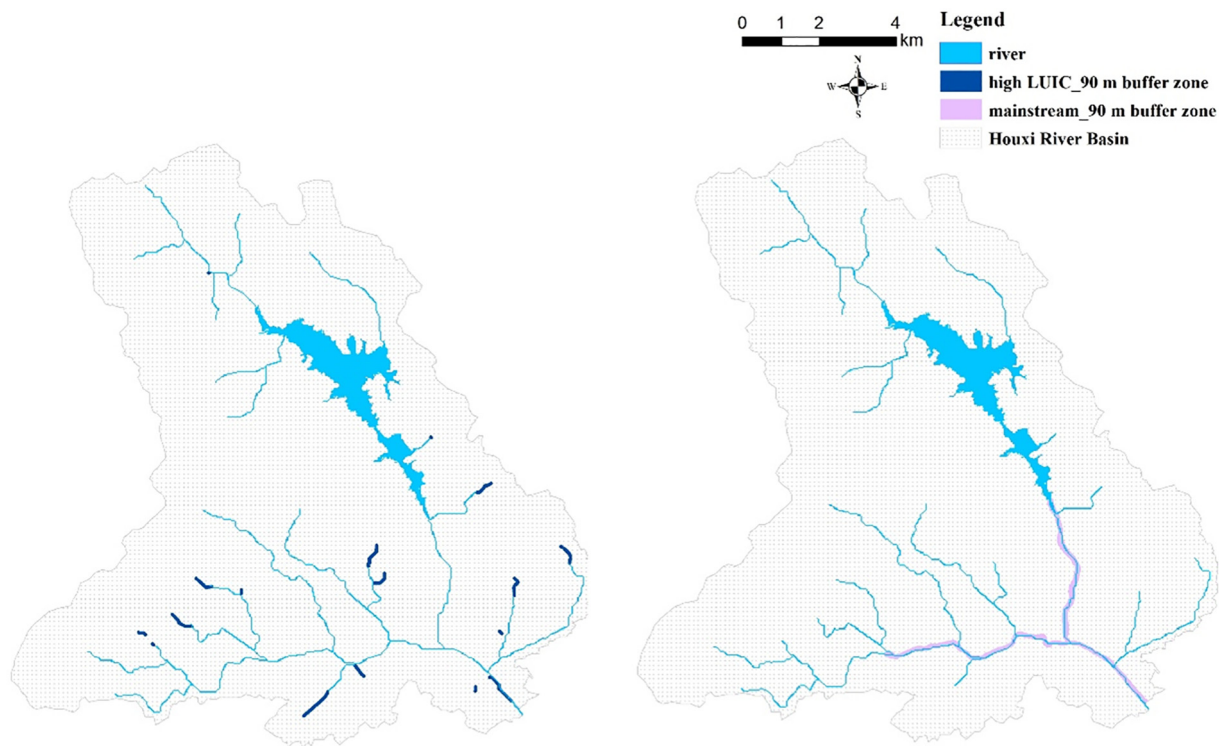


Fig. 3. Distribution of 90-meter buffer zones in areas with high LUIC and mainstream of the Houxi River.

images were acquired from Google Earth (resolution 1.19 m) and the SPOT 6 satellite (resolution 1.5 m). (2) Based on visual interpretation of these images, land use/land cover images of the HRB were obtained for 2011, 2015, and 2019. The land use/land cover can be divided into nine types, including forest land, grassland, orchard, cultivated land, rural residential area, construction land, ponds, bare land, and water body. (3) Based on the digital water system extracted from the DEM (ASTER GDEM, resolution 30 m), topographic and hydrological data such as watershed boundaries, river information, and slope can be extracted by processing these data using the ArcGIS 10.2.2 software (Esri, Redlands, CA, USA). (4) The rainfall data were hourly data from 25 rainfall monitoring points operated by the Xiamen Water Information Network (<http://sl.xm.gov.cn/>), and the IDW method was used to perform rainfall interpolation. (5) The soil data were sampling data. The HRB was divided into 4×4 km sized grids, and we selected one sample site from each grid. Then, we analyzed the soil grain diameter. (6) EC and LUIC were simulated using Python and were presented using ArcGIS 10.2.2.

4. Results and analyses

4.1. Spatial distribution of LUIC

Overall, it was found that the spatial distributions of the LUIC for five intervals were relatively similar in 2011, 2015, and 2019. However, the extent of areas with high LUIC increased slightly between 2011 and 2019, as shown in Fig. 6. Meanwhile, the extent of areas with low LUIC decreased from 95.51% in 2011 to 95.10% in 2019. The extent of areas with medium-to-low LUIC increased from 3.00% in 2011 to 3.19% in 2019; the extent of areas with medium LUIC increased from 0.88% in 2011 to 0.92% in 2019; the extent of areas with medium-to-high LUIC increased from 0.44% in 2011 to 0.49% in 2019; and the extent of areas with high LUIC increased from 0.17% in 2011 to 0.30% in 2019.

In terms of LUIC distributed in different land use/land cover types, areas with high LUIC in the HRB mainly coincided with construction

land or bare land (Fig. 7). Therefore, optimizing the land use/land cover of key regions, such as areas with high LUIC, is an effective way to reduce the EC and control NPS pollution in watersheds.

4.2. ECs of land use scenario simulations

4.2.1. Comparison of ECs in the mainstream of the Houxi River and areas with high LUIC

When making a 90-meter buffer zone along the mainstream of the Houxi River, the buffer area is 1.16 km², and the EC decreased by 0.21% in the whole HRB between 2011 and 2019. When making a 90-meter buffer zone along areas with high LUIC, the buffer area is 0.71 km², and the EC decreased by 0.58% in the whole HRB between 2011 and 2019, as shown in Fig. 8. The results show that, compared with the buffer zone in the mainstream of the river, by optimizing land use/land cover types and spatial distributions of areas with high LUIC, the decline rate of the EC is higher.

4.2.2. Analysis of ECs under a 90-meter buffer zone for different LUIC values

Buffer zone analysis was carried out for a 90-meter buffer zone with different LUIC values, and the ECs in the whole HRB were reduced to varying degrees between 2011 and 2019, as shown in Fig. 9. (1) When making a 90-meter buffer zone around areas with high LUIC, the buffer zone area was 0.71 km² and the EC decreased by 0.58%. (2) When making a 90-meter buffer zone around areas with medium-to-high LUIC, the buffer zone area was 1.65 km² and the EC decreased by 1.14%. (3) When making a 90-meter buffer zone around areas with medium LUIC, the buffer zone area was 3.25 km² and the EC decreased by 1.74%. (4) When making a 90-meter buffer zone around areas with medium-to-low LUIC, the buffer zone area was 7.85 km² and the EC decreased by 2.64%.

Regarding sub-watersheds, when ECs are estimated under different LUIC values (90-meter buffer zone), the 21st sub-watershed has the highest decrease in EC, followed by the 24th sub-watershed and the

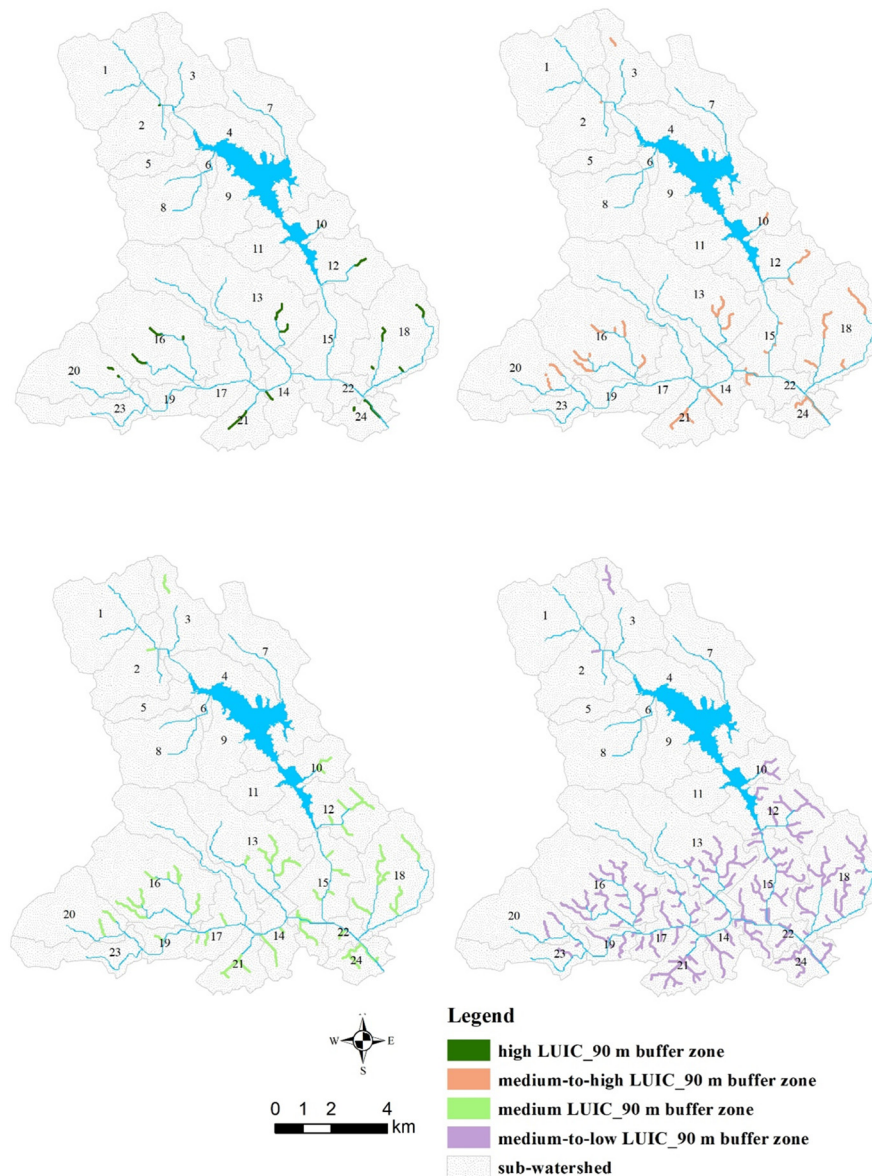


Fig. 4. Distribution of 90-meter buffer zones in areas with different LUIC values.

15th sub-watershed, as shown in Fig. 10. These sub-watersheds are all near the mainstream of the Houxi River.

In the 21st sub-watershed, (1) when making a 90-meter buffer zone around areas with high LUIC in the sub-watershed, the buffer zone area was 0.09 km² and the EC decreased by 5.00%, (2) when making a 90-meter buffer zone around areas with medium-to-high LUIC in the sub-watershed, the buffer zone area was 0.14 km² and the EC decreased by 5.86%, (3) when making a 90-meter buffer zone around areas with medium LUIC in the sub-watershed, the buffer zone area was 0.17 km² and the EC decreased by 6.22%, (4) when making a 90-meter buffer zone around areas with medium-to-low LUIC in the sub-watershed, the buffer zone area was 0.55 km² and the EC decreased by 9.98%.

4.2.3. Analysis of ECs under different buffer zone widths in areas with high LUIC

The effect of the buffer zone width in areas with high LUIC was studied, and the ECs in the whole basin were reduced to varying degrees between 2011 and 2019, as shown in Fig. 11. (1) when making a 90-meter buffer zone in areas with high LUIC, the buffer zone area was 0.71 km² and the EC decreased by 0.58%, (2) when making a 150-meter buffer zone in areas with high LUIC, the buffer zone area was 1.13 km² and

the EC decreased by 0.80%, (3) when making a 300-meter buffer zone in areas with high LUIC, the buffer zone area was 2.74 km² and the EC decreased by 1.07%, (4) when making a 600-meter buffer zone in areas with high LUIC, the buffer zone area was 7.13 km² and the EC decreased by 1.70%, and (5) when making a 1000-meter buffer zone in areas with high LUIC, the buffer zone area was 14.24 km² and the EC decreased by 2.46%.

Regarding sub-watersheds, when ECs were estimated under different buffer zone widths in areas with high LUIC, the 21st sub-watershed has the highest decrease in EC, followed by the 24th sub-watershed and the 14th sub-watershed, as shown in Fig. 12. All of these sub-watersheds are located near the mainstream of the Houxi River.

In the 21st sub-watershed, (1) when making a 90-meter buffer zone in areas with high LUIC in the sub-watershed, the buffer zone area was 0.09 km² and the EC decreased by 5.00%, (2) when making a 150-meter buffer zone in areas with high LUIC in the sub-watershed, the buffer zone area was 0.15 km² and the EC decreased by 5.79%, (3) when making a 300-meter buffer zone in areas with high LUIC in the sub-watershed, the buffer zone area was 0.36 km² and the EC decreased by 6.96%, (4) when making a 600-meter buffer zone in areas with

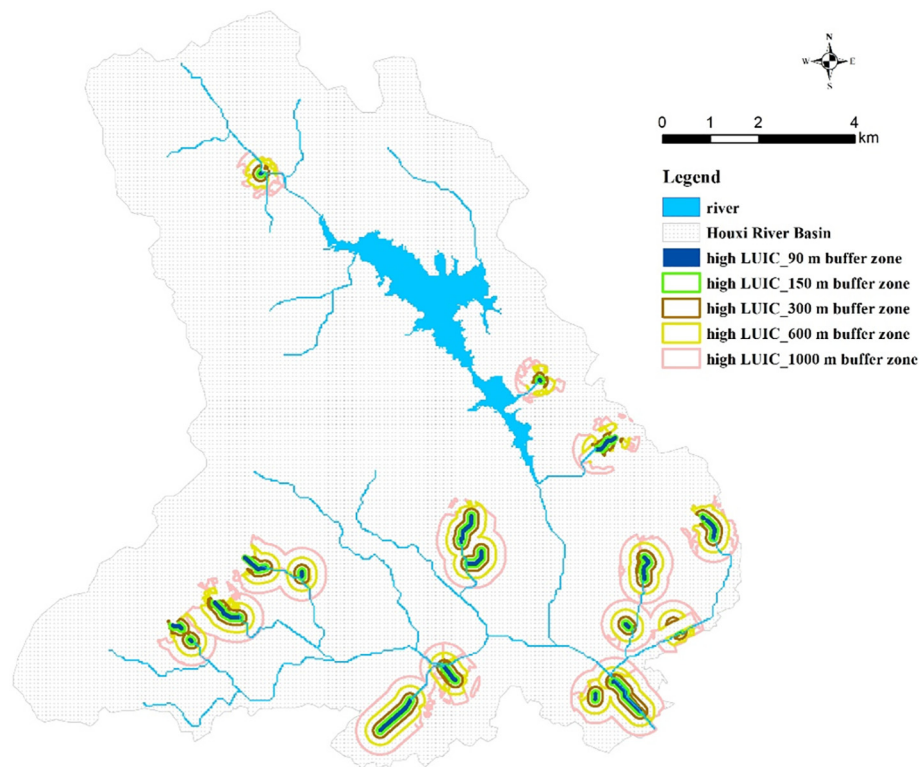


Fig. 5. The distribution of buffer zones of different widths in areas with high LUIC values.

high LUIC in the sub-watershed, the buffer zone area was 0.96 km² and the EC decreased by 9.70%, and (5) when making a 1000-meter buffer zone in areas with high LUIC in the sub-watershed, the buffer zone area was 1.89 km² and the EC decreased by 14.73%.

4.3. Comparison of decline rates of ECs by optimizing the same/similar areas with high LUIC

We compared the degree of reduction of the ECs in the sub-watersheds whose areas of land use/land cover change were about 0.05 (± 0.01) km², 0.10 (± 0.01) km², 0.15 (± 0.02) km², 0.20 (± 0.04) km², 0.50 (± 0.04) km², and 1.00 (± 0.2) km², as shown in Fig. 13. When the area of land use/land cover change was 0.05 (± 0.01) km², the reduction of EC in the 21st sub-watershed is particularly large, at 2.18%. When the area of land use/land cover change was 0.1 (± 0.01) km², the reduction of EC in the 12th sub-watershed was also particularly large, at 3.05%, while the reduction of EC in the 3rd sub-watershed was the lowest, at 0.15%. When the area of land use/land cover change was 0.15 (± 0.02) km², the reduction of EC in the 21st sub-watershed was particularly large, at 5.79%. When the area of land use/land cover change was 0.20 (± 0.04) km², the reduction of EC in the 12th sub-watershed was also particularly large, at 3.30%; meanwhile, the reduction of EC in the 16th and 20th sub-watersheds was less than 1% and that in the 2nd and 13th sub-watersheds was less than 1.5%. When the area of land use/land cover change was 0.50 (± 0.04) km², the reduction of EC in the 14th sub-watershed was particularly high, at 6.68%, while that in the 20th sub-watershed was 0.84%. When the area of land use/land cover change was 1.00 (± 0.2) km², the reduction of EC in the 21st and 24th sub-watersheds was particularly large, at 9.70% and 6.37%, respectively. This shows that optimizing the land use/land cover in sub-watersheds close to the mainstream of the river can significantly reduce the EC, while optimizing the land use/land cover in sub-watersheds far from the mainstream of the river may do little to reduce NPS pollution entering the water body. In sum, the closer the sub-watershed is to

the mainstream, the more effective the reduction of EC by optimizing land use/land cover in areas with high LUIC.

5. Discussion

5.1. Optimizing land use/land cover in the key areas has a better effect for preventing pollutants from entering the river

Based on the results of Section 4.2.3, it was found that the larger the buffer zone area is, the higher the decline rate of the ECs. However, the larger the buffer zone area, the higher the greening costs. Therefore, we compared the decline rate of ECs under the two scenes, including areas with the four LUIC values and different buffer zones widths in areas with high LUIC. On the whole, the ECs under the four LUIC values had a higher decline rate between 2011 and 2019, as shown in Figs. 9 and 11. It was found that it is more effective to optimizing land use/land cover in the key areas for preventing pollutants from entering the river, other than greening larger buffer zones.

Most sub-watersheds show the same situation as the whole basin. That is, compared with the ECs of the areas with high LUIC under different buffer zone widths in most sub-watersheds, the ECs of the areas with high LUIC under different buffer zone widths have a higher decline rate between 2011 and 2019. For example, when a 90-meter buffer zone is implemented in the medium-impact area in the 3rd sub-watershed, it occupied 1.35% of the area of the sub-watershed, and the EC decreased by 0.68%. Meanwhile, when a 1000-meter buffer zone was created for the high-impact area of the 3rd sub-watershed, it occupied 1.73% of the area of the sub-watershed and the EC only decreased by 0.15%. When a 90-meter buffer zone is implemented in the medium-to-low impact area in the 21st sub-watershed, it accounts for 15.12% of the area of the sub-watershed and the EC decreased by 9.98%. Meanwhile, when a 600-meter buffer zone was created for the high-impact area of the 21st sub-watershed, it occupied up to 26.36% of the area of the sub-watershed and the EC decreased by 9.70%.

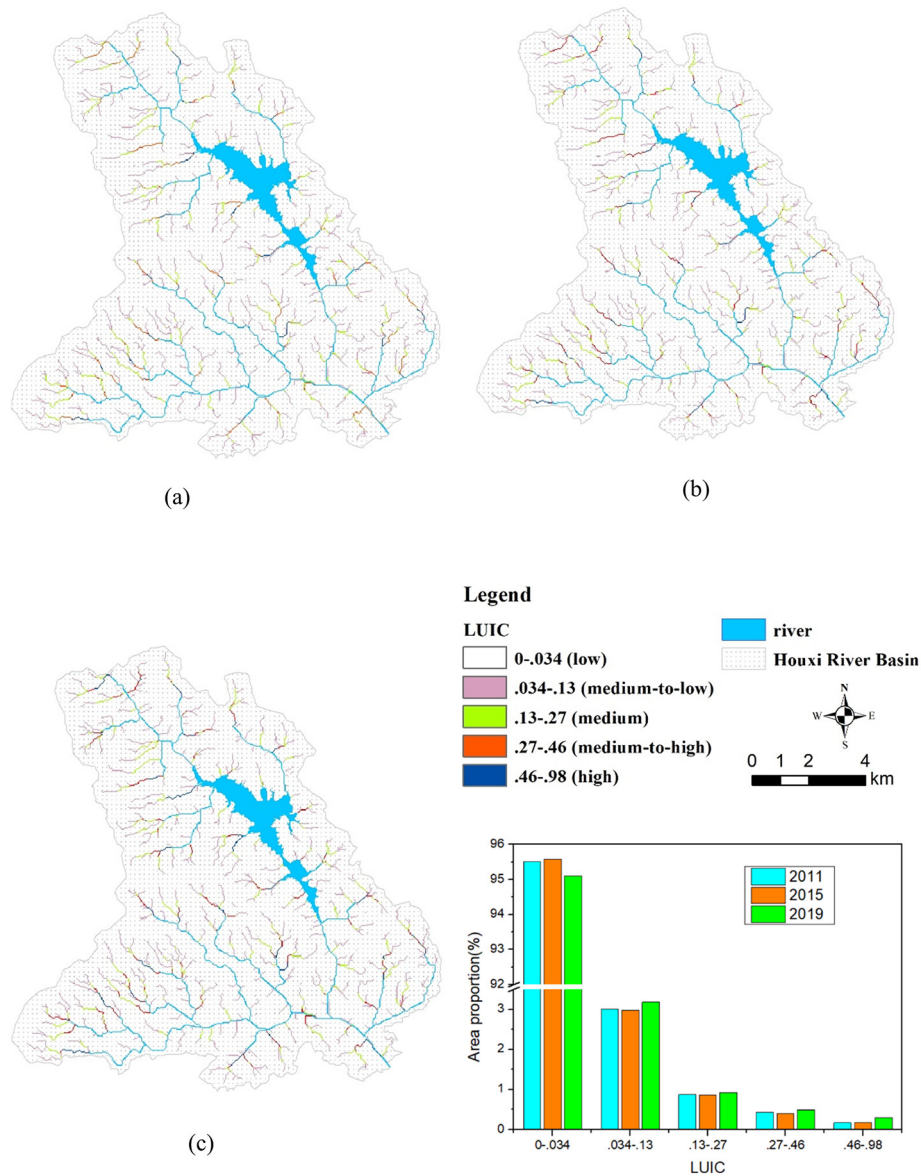


Fig. 6. LUIC distribution in the HRB in (a) 2011, (b) 2015, and (c) 2019.

In our study, when the selection range of the LUIC is the medium-impact and above, most sub-watersheds have a significant decrease in the EC between 2011 and 2019. However, it is also necessary to consider the actual situation of the sub-watersheds; that is, it is not appropriate to blindly pursue the reduction of pollution (i.e., the maximum decline rate of EC). Additionally, it is important to reduce greening costs by controlling the areas of buffer zones. For example, when making a 90-meter buffer zone around the medium-to-high impact areas in the 10th sub-watershed, the buffer zone area occupied 0.93% of the area of the sub-watershed and the EC decreased by 1.06%; meanwhile, when making a 90-meter buffer zone around the medium-to-low impact areas, the buffer zone occupied up to 3.97% of the area of the sub-watershed and the EC decreased by 1.08%. Therefore, the former has more advantages in reducing EC than the latter.

5.2. Optimizing land use/land cover changes in a certain sub-watershed can reduce the EC to adjacent or downstream sub-watersheds

Based on the results of Section 4.2.2, it was found that, although there are no areas with high LUIC in the 15th sub-watershed, when a

90-meter buffer zone is implemented in the areas with high LUIC around the 15th sub-watershed (including the 12th, 13th, 14th, and 18th sub-watersheds), the EC of the 15th sub-watershed reduced to a small extent (0.003%).

A similar observation was made for the 23rd sub-watershed. Although there are no areas with medium-to-high LUIC, or areas with medium LUIC in this sub-watershed, the EC of the sub-watershed is affected when a buffer zone is implemented in the 20th sub-watershed, which is located upstream of the 23rd sub-watershed. When making a 90-meter buffer zone in the areas with medium-to-high LUIC in the 20th sub-watershed (0.11 km²), the EC of the 23rd sub-watershed was reduced by 0.01%.

This shows that, when implementing a buffer zone (that is, to optimize land use/land cover changes) in certain sub-watersheds, the EC of adjacent or downstream sub-watersheds can be reduced.

5.3. Compared with nutrient delivery ratio model (NDR)

NDR is one of models in Integrated Valuation of Ecosystem Services and Tradeoffs (InVEST) which focusing on evaluating NPS pollution

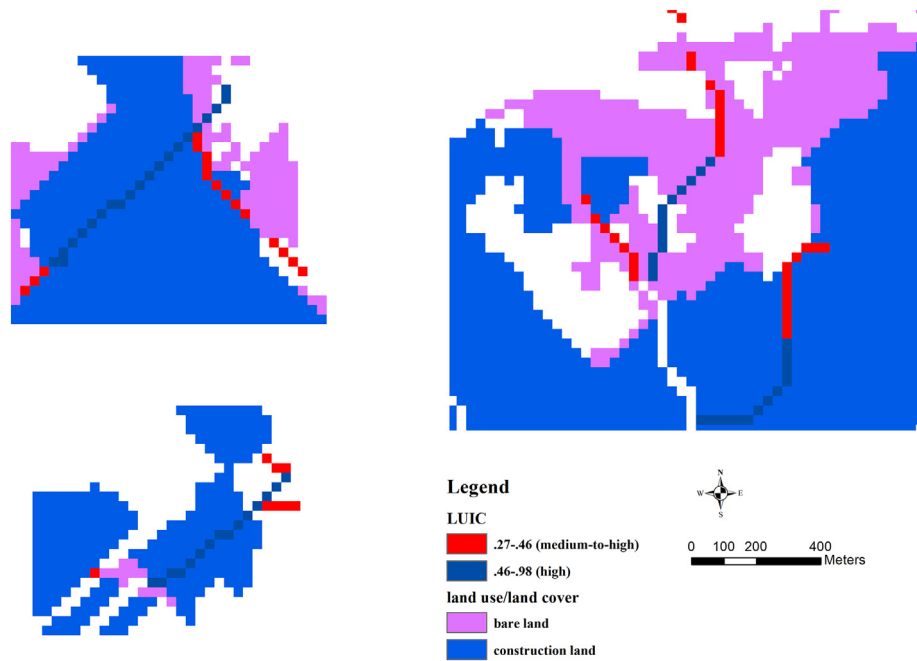


Fig. 7. LUIC distribution (high LUIC and medium-to-high LUIC) corresponding to land use/land cover (construction land and bare land).

loads (Terrado et al., 2014). Both NDR and our model reflects highly simplified ecological process of NPS pollution transport and retention, and the similarity is sources of nutrients are defined by land use/land cover and results can fall on the pixel scale. The biggest difference between NDR and our model is that the export results instead of being estimated by NPS pollution loads are defined by the proportion of NPS pollution. Because if calibration data is hardly available, the absolute value of the loads need to be use with caution. Despite that both models can reflect the contributions of land use/land cover on NPS pollution, our study

furtherly extracted the land use impact coefficient which intuitively reflects the response of land use change to the migration of NPS pollution.

6. Conclusions

The reasonable planning of the spatial layout of green space is an important way to alleviate the non-point source pollution entering rivers. In our study, we found that not all export coefficients of NPS pollution of

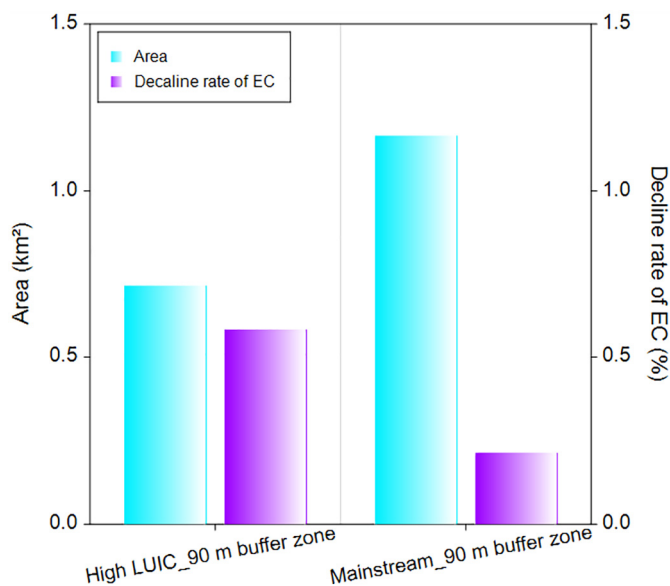


Fig. 8. Comparisons of the area and the decline rate of EC between 2011 and 2019 in the mainstream of the Houxi River with a 90-meter buffer zone and areas with high LUIC with a 90-meter buffer zone.

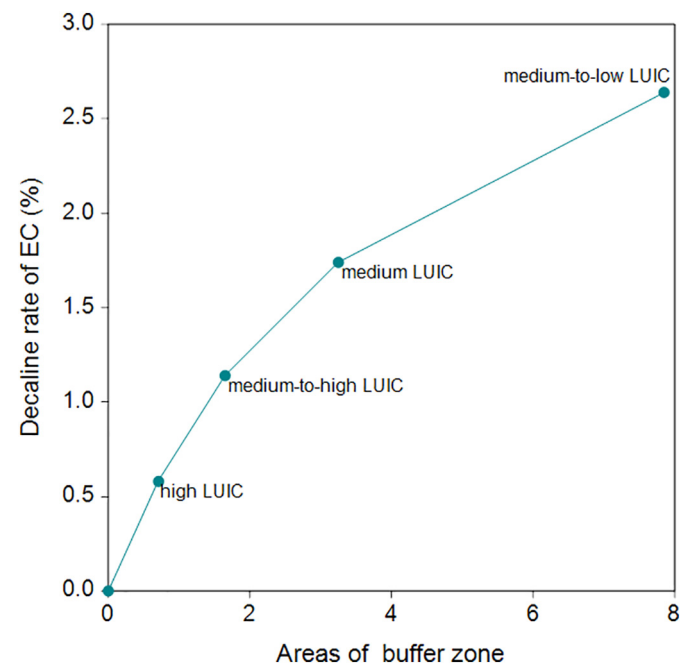


Fig. 9. The decline rate of the ECs in the whole HRB between 2011 and 2019 for 4 LUIC values (90-meter buffer zone).

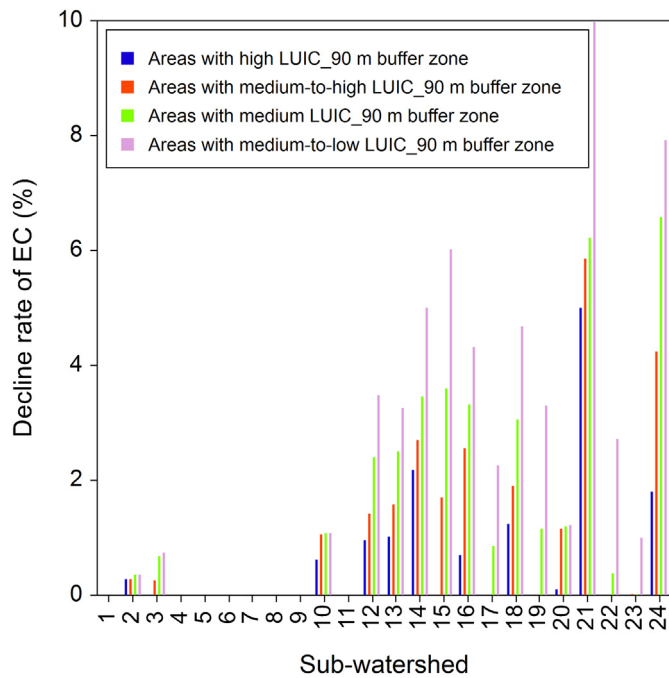


Fig. 10. The decline rate of the EC between 2011 and 2019 in each sub-watershed under different LUIC values (90-meter buffer zone).

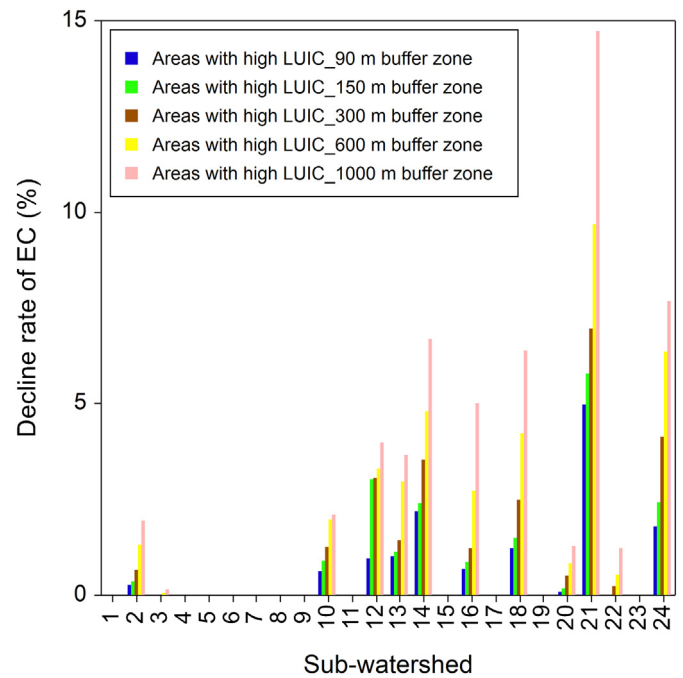


Fig. 12. The decline rate of the EC in each sub-watershed of the HRB between 2011 and 2019 under different buffer zone widths in areas with high LUIC.

the riverside plots are high. Besides, the larger the buffer zone area, the higher the greening costs. Furthermore, it is unclear whether the environmental benefit outweighs the economic cost, if all the greening area along the river is reconstructed in accordance with the traditional buffer zone method.

Therefore, we proposed a key indicator—the land use impact coefficient—which can effectively identify the key areas that cause pollution entering the water body to select targeted measures (land management, spatial planning, etc.) to effectively reduce the risk to aquatic

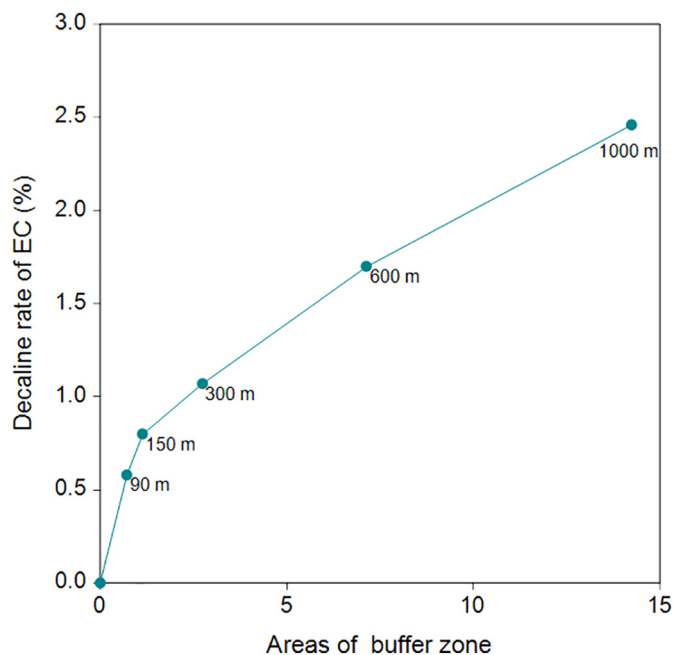


Fig. 11. The decline rate of the ECs in the whole HRB between 2011 and 2019 under different buffer zone widths in areas with high LUIC.

ecosystem at a lower cost. By reorganizing and optimizing the land use/land cover or landscape pattern in key areas, the export coefficients of different sub-watersheds can be reduced to reduce the amount of NPS pollution entering the water body. In our research, when greening areas with high land use impact coefficient are 0.71 km², the decline rate of export coefficients (0.58%) is higher than optimizing land use/land cover types of areas along the mainstream of the river, for export coefficients reduced by 0.21% with the greening areas of 1.16 km².

The advantage of the proposed method is that it simplifies complex ecological processes and intuitively simulates the path of NPS pollution from the surface to the water body. Besides, the results of the method can help to alleviate the watershed pollution caused by human activities by optimizing the land use/land cover in specific areas when other conditions are stable. The limitation of this research is that different pollutants follow different attenuation patterns during the migration process. Therefore, in future work, we plan to improve and modify the method accordingly.

Funding

This work was supported by the Crossing-Group Projects of the Chinese Academy of Sciences Key Laboratory of Urban Environment and Health (KLUEH-C-201801) and the National Key R&D Program of China (2016YFC0502902).

CRedit authorship contribution statement

Yao Qian: Conceptualization, Methodology, Writing – original draft. **Lang Sun:** Data curation, Software. **Dingkai Chen:** Software, Validation. **Jiangfu Liao:** Visualization. **Lina Tang:** Writing – review & editing, Supervision. **Qian Sun:** Investigation.

Declaration of competing interest

The authors declare that they have no known competing financial interests or personal relationships that could have appeared to influence the work reported in this paper.

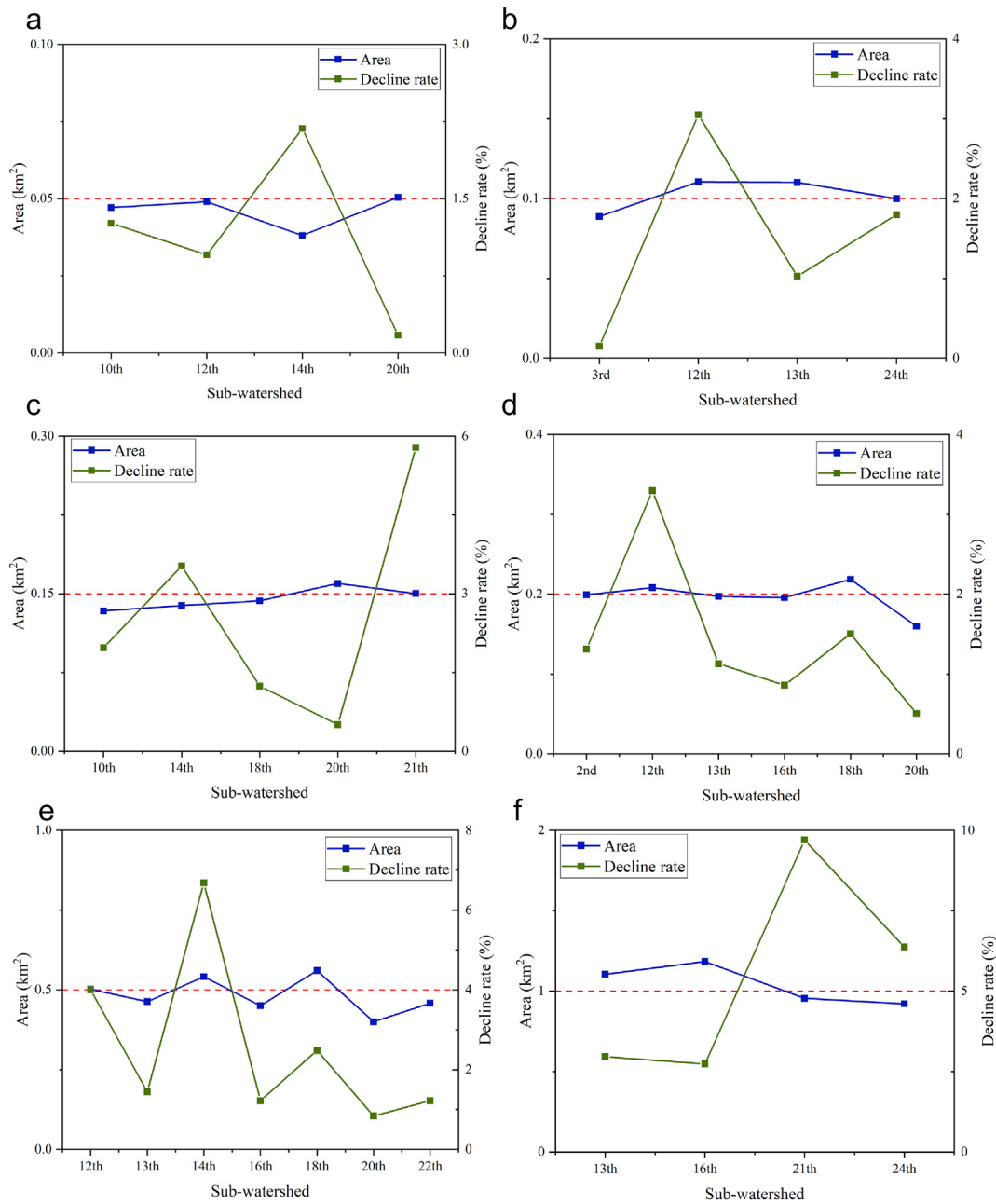


Fig. 13. The degree of reduction of ECs in the sub-watersheds between 2011 and 2019 with the same or similar areas of land use/land cover change. (a) 0.05 (± 0.01) km². (b) 0.10 (± 0.01) km². (c) 0.15 (± 0.02) km². (d) 0.20 (± 0.04) km². (e) 0.50 (± 0.04) km². (f) 1.00 (± 0.2) km².

References

Beaulac, M.N., Reckhow, K.H., 1982. An examination of landuse-nutrient export relationships. *Water Resour. Bull.* 18, 1013–1024.

Chen, L., 2015. *Source-Sink Landscape Pattern Analysis and Its Application*. Science Press, Beijing ISBN 978-7-03-046762-1.

Dai, X., Zhou, Y., Ma, W., Zhou, L., 2017. Influence of spatial variation in land-use patterns and topography on water quality of the rivers inflowing to Fuxian Lake, a large deep lake in the plateau of southwestern China. *Ecol. Eng.* 99, 417–428.

Ervinia, A., Huang, J., Huang, Y., Lin, J., 2019. Coupled effects of climate variability and land use pattern on surface water quality: an elasticity perspective and watershed health indicators. *Sci. Total Environ.* 693. <https://doi.org/10.1016/j.scitotenv.2019.133592>

Fu, X., Cao, W., Cao, Y., Pan, K., 2005. Change of land-use and environmental effect in peri-urbanization region: a case study of Xinjin county in Chengdu. *China Popul. Resour. Environ.* 15 (3), 80–83.

Hodge, T.A., Armstrong, L.J., 1993. Use of a multiple linear regression model to estimate stormwater pollutant loading. In: James, W. (Ed.), *New Techniques for Modelling the Management of Stormwater Quality Impacts*. Lewis Publishers, Boca Raton, Florida, pp. 201–214.

Huang, Y., Cui, S., Shi, L., 2012. Response of ecosystem services to land use/land cover change in peri-urban area: a case study of Jimei district, Xiamen. *Prog. Geogr.* 31 (5), 551–560 in Chinese.

Johnes, P.J., 1996. Evaluation and management of the impact of landuse change to the nitrogen and phosphorus load delivered to surface waters: the export coefficient modelling approach. *J. Hydrol.* 183, 323–349.

Liang, K., Jiang, Y., Qi, J., Fuller, K., Nyiraneza, J., Meng, F., 2020. Characterizing the impacts of land use on nitrate load and water yield in an agricultural watershed in Atlantic Canada. *Sci. Total Environ.* 729. <https://doi.org/10.1016/j.scitotenv.2020.138793>

Liu, S., Chen, T., Cai, J., 2004. Peri-urbanization in China and its major research issues. *Acta Geograph. Sin.* 59, 101–108 in Chinese.

Loehr, R.C., Ryding, S.O., Sonzogni, W.C., Ryding, S.O., Rast, W., 1989. *Estimating the nutrient load to a water body. The Control of Eutrophication of Lakes and Reservoirs. Man and the Biosphere Series Vol. I*. United Nations Educational Scientific and Cultural Organization, Paris, France and The Parthenon Publishing Group, Park Ridge, NJ, pp. 115–146.

McFarland, A., Hauck, L., 1998. *Determining nutrient contribution by land use for the Upper North Bosque River Watershed. Lake Waco/Bosque River Watershed Initiative Report*. <https://www.doc88.com/p-7773105751431.html> (accessed 18 March 2020).

- Munafò, M., Cecchi, G., Baiocco, F., Mancini, L., 2005. River pollution from non-point source: a new simplified method of assessment. *J. Environ. Manag.* 77 (2), 93–98.
- Ongley, E.D., Zhang, X., Yu, T., 2010. Current status of agricultural and rural non-point source pollution assessment in China. *Environ. Pollut.* 158 (5), 1159–1168.
- Shrestha, S., Kazama, F., 2006. Estimation of organic matter and nutrient loadings from point and nonpoint sources into the Fuji River, Japan: export coefficient modeling approach. *International Congress on Environmental Modelling and Software*. 365.
- Shrestha, S., Kazama, F., Newham, L.T.H., 2008. A framework for estimating pollutant export coefficients from long-term in-stream water quality monitoring data. *Environ. Model. Softw.* 23 (2), 182–194.
- Sun, R., Chen, X., Chen, L., 2018. A precipitation-weighted landscape structure model to predict potential pollution contributions at watershed scales. *Landsc. Ecol.* 33, 1603–1616.
- Tang, L., Wang, L., Li, Q., Zhao, J., 2018. A framework designation for the assessment of urban ecological risks. *Int. J. Sustain. Dev. World Ecol.* 25 (5), 387–395.
- Terrado, M., Acuña, V., Ennaanay, D., Tallis, H., Sabater, S., 2014. Impact of climate extremes on hydrological ecosystem services in a heavily humanized Mediterranean basin. *Ecol. Indic.* 37, 199–209.
- Wang, K., Wang, P., Zhang, R., Lin, Z., 2019. Determination of spatiotemporal characteristics of agricultural non-point source pollution of river basins using the dynamic time warping distance. *J. Hydrol.* <https://doi.org/10.1016/j.jhydrol.2019.124303>.
- White, M., Harmel, D., Yen, H., Arnold, J., Gambone, M., Haney, R., 2015. Development of sediment and nutrient export coefficients for U.S. ecoregions. *J. Am. Water Resour. Assoc.* 51 (3), 758–775.
- Xie, H., Du, J., Hu, Y., Wu, C., Yan, W., 2005. Study on spatially distributed hydrological model based on routing time method. *J. Wuhan Univ. Technol.* 12, 75–78 in Chinese.
- Xu, Z., 2009. *Hydrological Models*. Science Press, Beijing.
- Yan, Y., Qian, Y., Wang, Z., Yang, X., Wang, H., 2018. Ecological risk assessment from the viewpoint of surface water pollution in Xiamen City, China. *Int. J. Sustain. Dev. World Ecol.* 25 (5), 403–410.
- Zhang, P., Liu, Y., Pan, Y., Yu, Z., 2013. Land use pattern optimization based on clue-s and swat models for agricultural non-point source pollution control. *Math. Comput. Modell.* 58, 588–595.
- Zhang, X., Zhou, L., Liu, Y., 2018. Modeling land use changes and their impacts on non-point source pollution in a southeast China coastal watershed. *Int. J. Environ. Res. Public Health* 15, 1593.
- Zhao, X., Chen, L., Yang, L., Ma, Y., Zhang, H., Shi, Q., 2010. Modeling non-point pollution based on interactions between flow path and landscape units. *Acta Sci. Circumst.* 30 (3), 621–630 in Chinese.